# Supporting information

# Synergistic Interface Engineering in $Bi_2O_3$-$In_2O_3$@CuO Nanowires for Highly Selective Electrocatalytic $CO_2$ Reduction to Formate

Rongtao Xiao, Ling Ma, Zhe Piao,Ya Zhang and Honggui Wang*

School of Environmental Science and Engineering, Yangzhou University, Yangzhou, Jiangsu, 225127, China.

*Corresponding author. E-mail: wanghg@yzu.edu.cn (H.G. Wang).

Phone: +86-15358512111.

**Physicochemical characterization:**

Morphological observations of the material were carried out on a field emission scanning electron microscope (SEM) (Hitachi S-4800). X-ray diffraction (XRD) patterns of samples were obtained on a Bruker D8 X-ray diffractometer with Cu Kα radiation (λ = 1.5406 Å) and a high-resolution transmission electron microscope (HRTEM) (Philips Tecnai G2 F30 S-TWIN) along with high-angle annular dark field scanning TEM (HAADF-STEM) and elemental mapping. X-ray photoelectron spectroscopy (XPS) measurements were measured on a Thermo Scientific X-ray photoelectron spectroscopy system (ESCALAB 250Xi) with monochromatic Al Kα Radiation (E=1486.2 eV), and the binding energies were calibrated by C 1s to 284.8 eV.

**Electrochemical characterization:**

All electrochemical tests were performed on a CHI660E electrochemical workstation (Chenhua, Shanghai, China). A proton exchange membrane (PEM, Nafion 117) was used as a separator for $CO_2$RR in an H-cell to avoid cross-product contamination. For the $CO_2$ reduction half-reaction, 0.5 M $KHCO_3$ solution was prepared as the electrolyte in a conventional H-cell, which utilized a three-electrode system including a modified working electrode, an Ag/AgCl reference electrode and a platinum sheet counter electrode. The volume of electrolyte in each cathode chamber was controlled to be 80 mL, and the effective contact area between the working electrode and the electrolyte was maintained at 1 $cm^2$.

Prior to performing individual electrochemical tests, high purity gases were passed into the solution for at least 40 minutes to ensure saturation. The pH of 0.5 M $KHCO_3$ saturated with argon was 8.7, and that of 0.5 M $KHCO_3$ saturated with carbon dioxide was 7.7. The gas flow rate was maintained at 20 sccm during the test by a Gas flow quality controller (IKFD-LC-300SCCM) (Aino Instrument Technology Co., Ltd (Beijing, Chin). To avoid chance, all electrochemical tests were performed in at least three sets of parallel experiments. All potentials measured in $CO_2$RR were converted to

reversible hydrogen electrodes (RHE): E(RHE) = E(Ag/AgCl) + 0.059×pH + 0.197 (V).

For the $CO_2$ reduction, linear scanning voltammetry (LSV) was measured in Ar and $CO_2$ saturated 0.5 M $KHCO_3$ at a sweep rate of 5 mV $s^{-1}$, respectively. $C_{dl}$ was calculated by varying sweep rates from 20 to 120 mV $s^{-1}$ in the potential range of -0.1 to 0.1 V (vs. RHE). The electrochemical impedance spectrum (EIS) was measured at a potential of -0.75 V (vs. RHE) with a frequency range of 0.01 Hz to 100 kHz and an amplitude of 5 mV.

**Calculation of FE, production rate (PR), single-pass conversion efficiency (SPCE), energy efficiency (EE) and electricity consumption**

The FE of liquid products for $CO_2$RR was calculated as follows:

$$FE = \frac{Q_{HCOOH^-}}{Q_{total}} \times 100\% = \frac{nZF}{it} \times 100\% \quad (1)$$

Here, Z is the number of transfer electrons to form 1 mol formate, 2 for $CO_2$RR. n is the moles of formate. F is Faraday constant (96,485 C $mol^{-1}$). $Q_{total}$ is number of charges transferred by the reaction.

The Faraday efficiency of gas product was calculated as follows:

$$FE = \frac{Q}{Q_{total}} \times 100\% = \frac{ZFV(mlmin^{-1}) \cdot v(vol\%) \cdot P(Pa)}{i(A)RT(K)} \times 100\% \quad (2)$$

For $CO_2$RR, Z = 2 is the number of transfer electrons to form 1 mol $H_2$ or CO. F is Faraday constant (96,485 C $mol^{-1}$). V is the gas flow rate (mL $min^{-1}$). v (vol%) is the volume concentration of CO or $H_2$ in the outlet gas. P is the pressure of the chromatography inlet ring (Pa). R is the ideal gas constant (8.314 J $mol^{-1}$ $K^{-1}$). T is the pressure of the chromatography inlet ring (K).

The PR (mmol $h^{-1}$ $cm^{-2}$) of formate produced by $CO_2$RR was calculated as follows:

$$PR = \frac{n}{t \times s} \times 100\% = \frac{C \times V}{t \times s} \times 100\% \quad (3)$$

where C (mmol $L^{-1}$) is the molar concentration of formate in the electrolyte. V (L) is the volume of the electrolyte, t (h) is the electrolysis time and S ($cm^2$) is the geometric area of the working electrode.

The SPCE for the conversion of $CO_2$ to formate was calculated as follows:

$$SPCE = \frac{\frac{Q \times FE}{ZF} \times 22.4(L\,mol^{-1})}{V\,(L\,min^{-1}) \times t\,(min)} = \frac{i \times FE \times 60\,(s\,min^{-1})}{ZF} \times \frac{22.4\,(L\,mol^{-1})}{V\,(L\,min^{-1})} \quad (4)$$

where Q (C) is the total charge through the system. V (L $min^{-1}$) is the $CO^2$ flow rate. t is the electrolysis time (min). Z is the number of transfer electrons to form 1 mol formate, and i is the recorded current (A).

The EE for the conversion of $CO_2$ to formate was calculated as follows:

$$EE = \frac{Energy_{required}}{Energy_{input}} = \frac{|E^{\theta}|}{E_{cell}} \times FE \quad (5)$$

Where $\Delta E^{\theta}$ (V) is the thermodynamic equilibrium potential of the specific product, F is the Faraday constant (96,485 C $mol^{-1}$), and $E_{Cell}$ (V) is the applied cell voltage.

Calculation of electricity consumption for formate production:

After 30 minutes of electrolysis, the consumed electricity (W) could be calculated according to the following equation:

$$W = U \times I \times t = U \times Q$$

where U is the applied cell voltage (V), I is the current (A), t is the electrolysis time (h), and Q is the total charge (C).

The quality of the formate could be calculated by the following formula:

$m = c \times V$

Here, V is the volume. the energy consumption per kilogram of formate was obtained as follow:

$$Energy\ consumption = \frac{W}{m} \quad (6)$$

## DFT calculations

All first-principles DFT calculations were conducted using the Vienma ab initio simulation package. It adopts the generalized gradient approximation in the Perdew−Burke−Ernzerhof functional (GGAPBE) to treat the electron exchange and correlation interaction while utilizing the projector-augmented wave method to describe the ion electron interactions. We applied a plane-wave basis set with a kinetic energy cut-off of 450 eV to perform the calculations. The orbital cutoff of 4.0 Å was used and the Γ-point and a 2 × 2 × 1 k-point mash were used to sample the Brillouin zones. For the CuO, a unit cell with 88 atoms was built, and a 20 Å vacuum space above the surface was created to separate the surface slab and its periodic image. All the molecules were placed in the same box of CuO. All calculations were conducted within the framework of spin-polarized DFT and the spin states were fully relaxed. The convergence criteria for the energy change, maximum force, and maximum displacement tolerances were set to $1.0 \times 10^{-5}$ Ha, 0.005 Ha/Å, and 0.005 Å, respectively. The free energy of each system is calculated by adding a Gibbs free energy correction, including contributions from zero-point energy (ZPE), enthalpy (H) and entropy (S) to the total energy calculated in Dmol$^3$. All the Gibbs free energy corrections were calculated in gas phase at 298.15 K. Each electrochemical reaction step during catalysis considered in the present work involves a ($H^+ + e^-$) pair transfer from the solution to the adsorbed species on the catalyst. All $Bi_2O_3$/CuO, $In_2O_3$/CuO and $Bi_2O_3$- $In_2O_3$/CuO supported systems were calculated under the standard pressure.

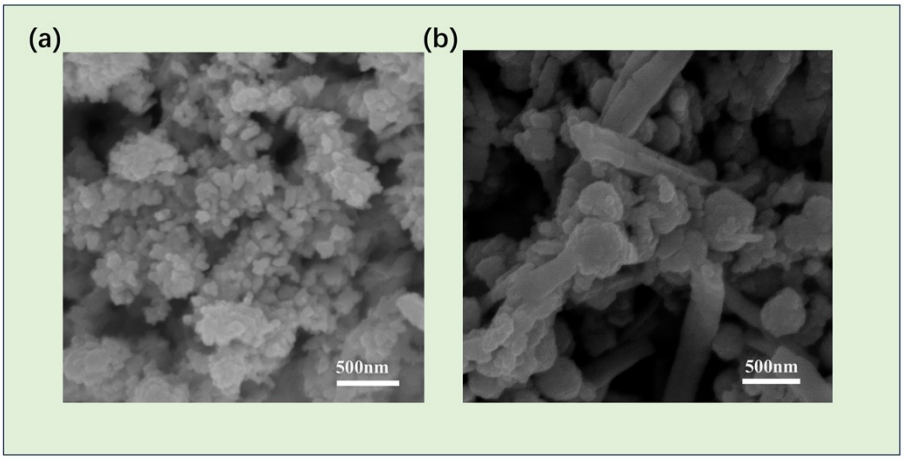


**Fig. S1** SEM images of (a) $Bi_2O_3$@CuO NWs and (b) $In_2O_3$@CuO NWs.

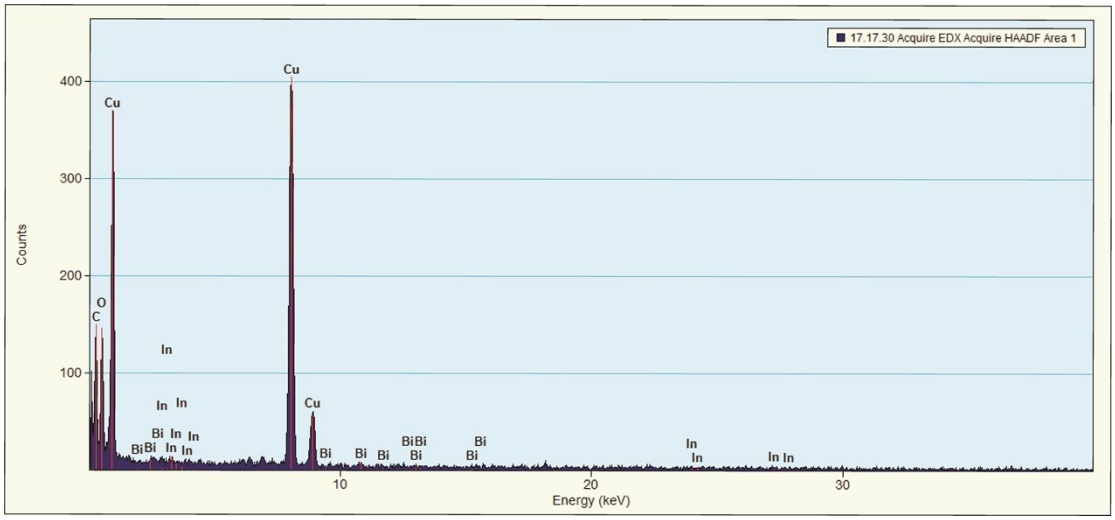


**Fig. S2** EDX spectrum of $Bi_2O_3$-$In_2O_3$@CuO NWs.

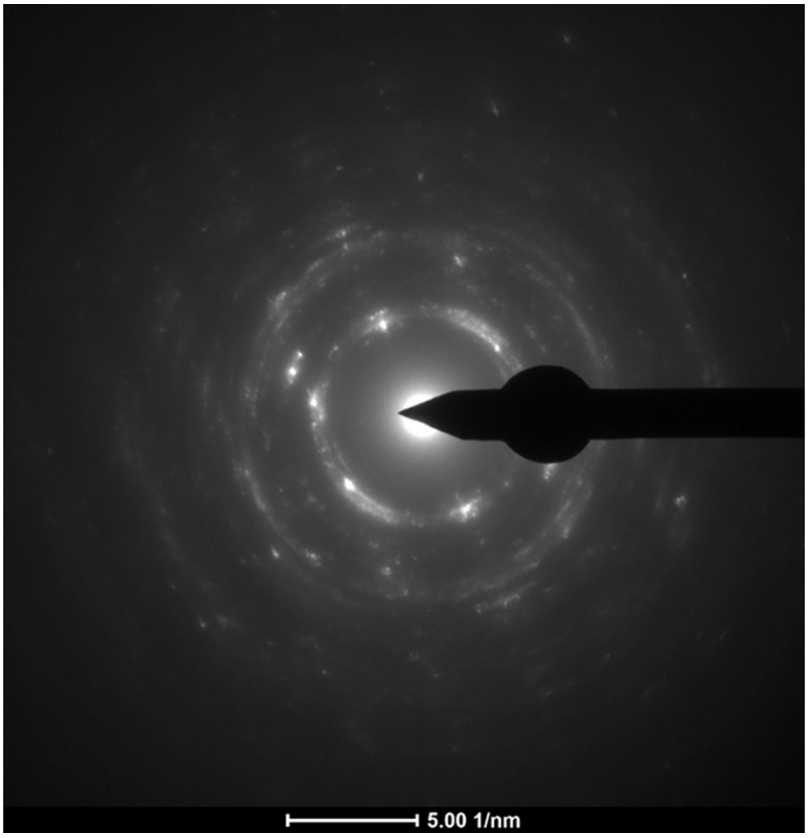


**Fig. S3** SAED image of $Bi_2O_3$-$In_2O_3$@CuO NWs.

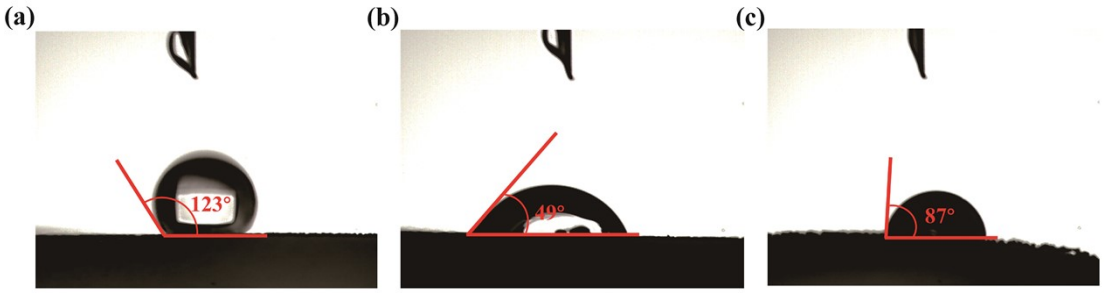


**Fig. S4** Contact angle test of (a) $Bi_2O_3$-$In_2O_3$@CuO NWs, (b) $Bi_2O_3$@CuO NWs and (c) $In_2O_3$@CuO NWs.

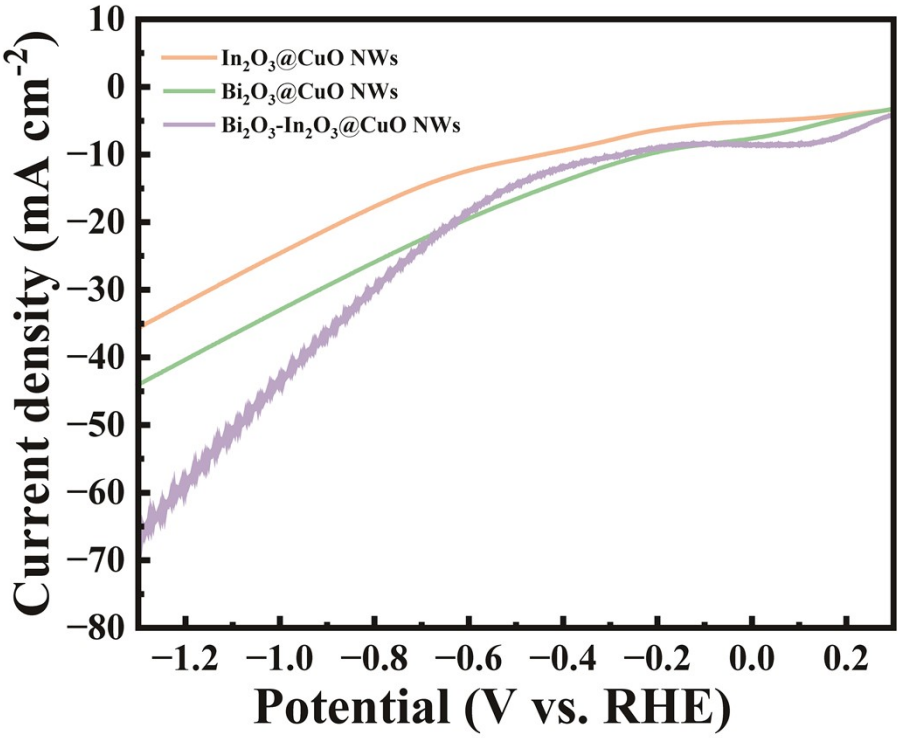


**Fig. S5** LSV curves of $Bi_2O_3$@CuO NWs, $In_2O_3$@CuO NWs and $Bi_2O_3$-$In_2O_3$@CuO NWs in $CO_2$-saturated 0.5 M $KHCO_3$ solution at scan rate of 5 mV $s^{-1}$.

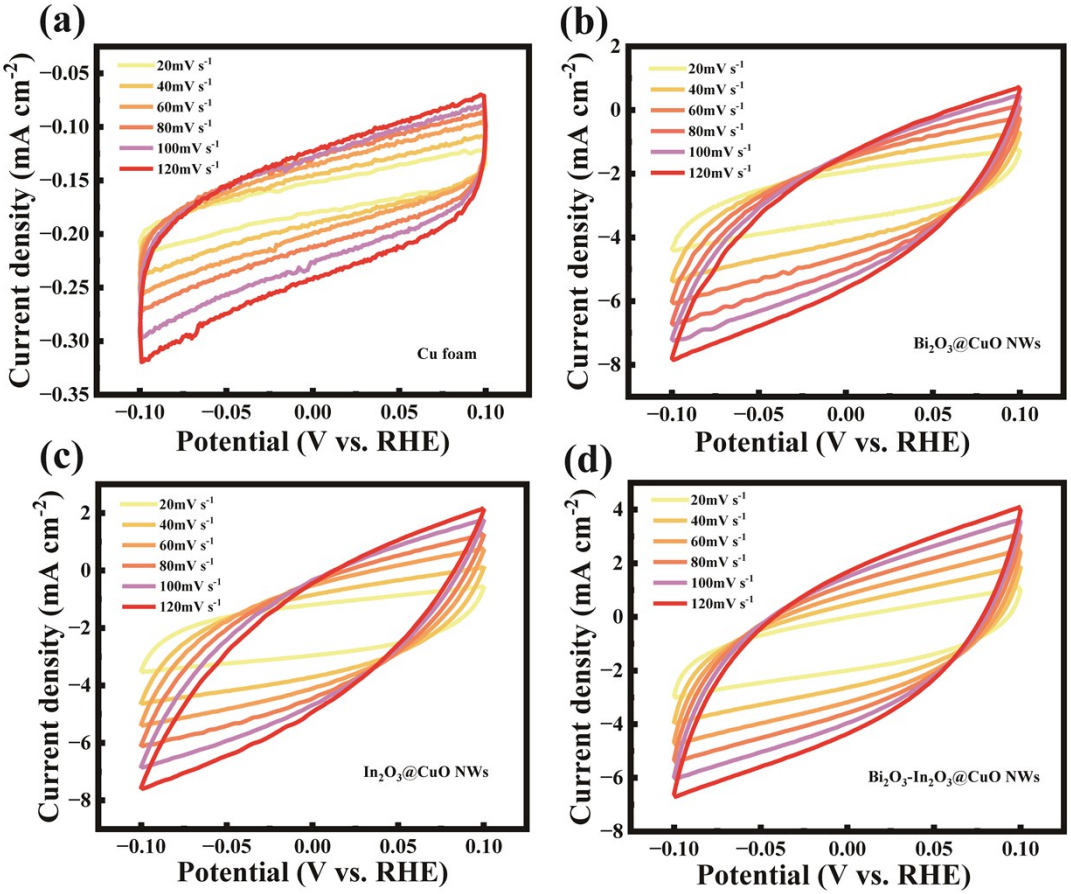


**Fig. S6** CV curves of (a) Cu foam, (b) $Bi_2O_3$@CuO NWs, (c) $In_2O_3$@CuO NWs and (d) $Bi_2O_3$-$In_2O_3$@CuO NWs from scan rate of 20 to 120 mV $s^{-1}$ in 0.5 M $KHCO_3$, potential ranges: -0.1 to 0.1 V (vs. RHE).

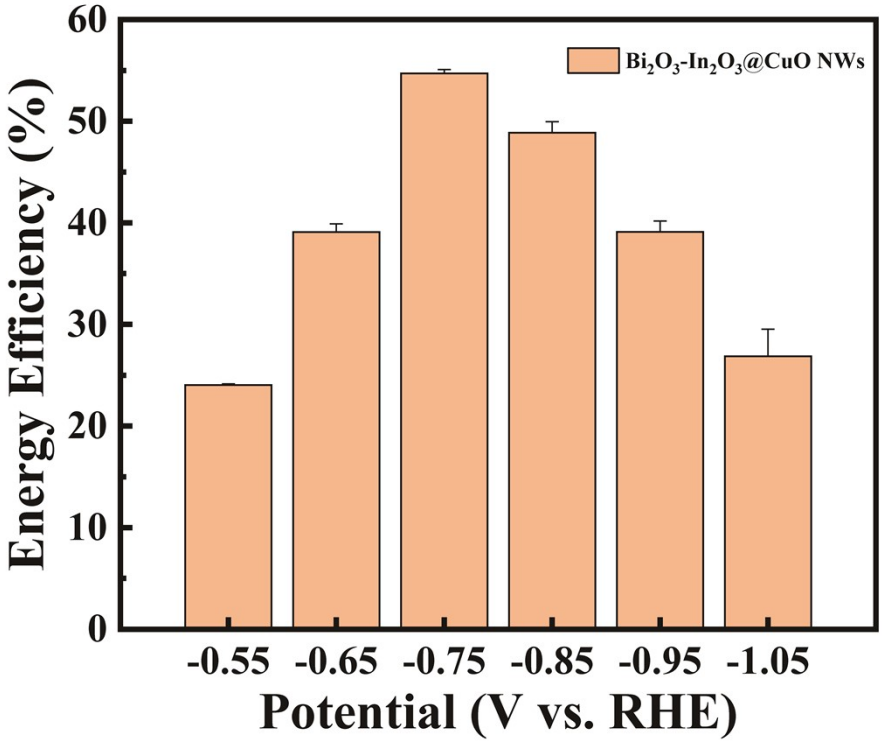


**Fig. S7** EE of $Bi_2O_3$-$In_2O_3$@CuO NWs for cathodic $CO_2$RR. Data are presented as mean ± SD (n=3).

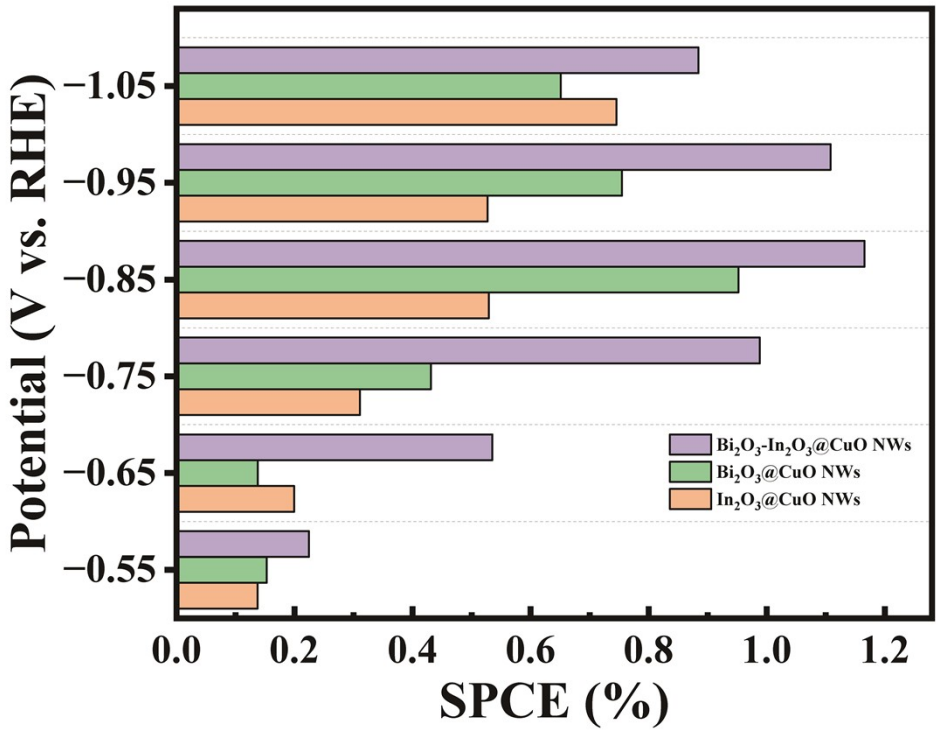


**Fig. S8** SPCE of $CO_2$ toward formate using $Bi_2O_3$-$In_2O_3$@CuO NWs, $Bi_2O_3$@CuO NWs and $In_2O_3$@CuO NWs.

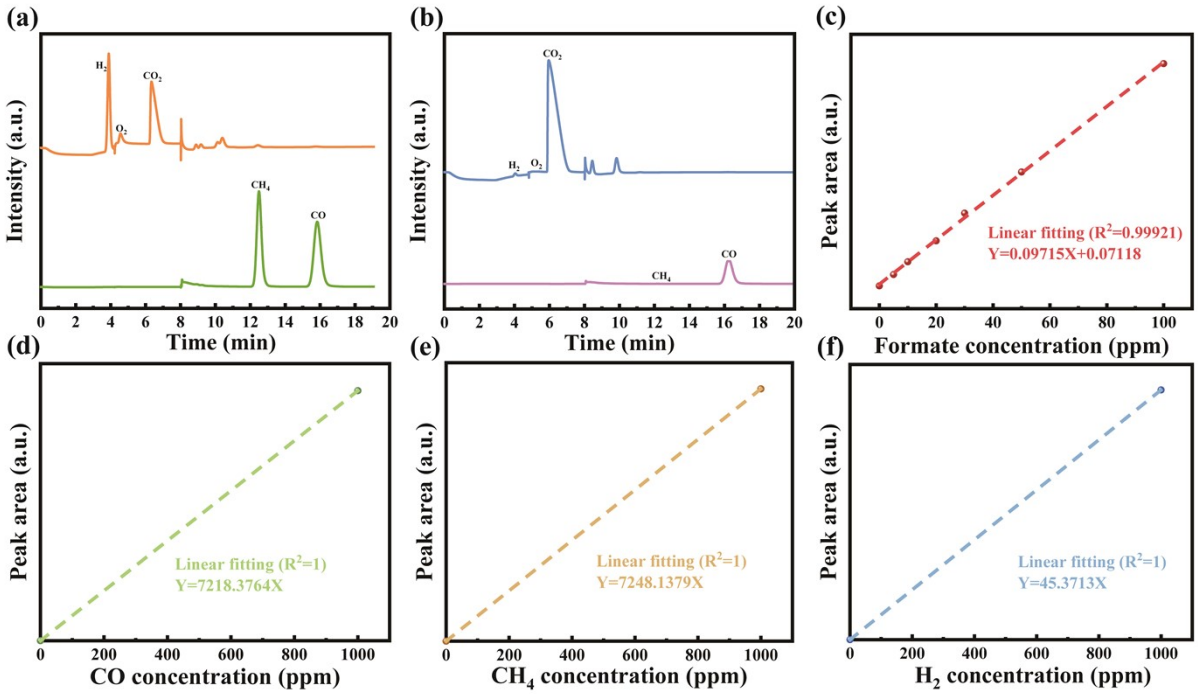


**Fig. S9** (a) GC spectrum of the mixed standard gas ($H_2$, CO, $CH_4$, et.al). (b) GC spectrum of the $Bi_2O_3$-$In_2O_3$@CuO NWs catalyst at -0.75 V (vs. RHE) electrochemical test in $CO_2$RR. Standard curves for (c) formate, (d) CO, (e) $CH_4$ and (f) $H_2$.

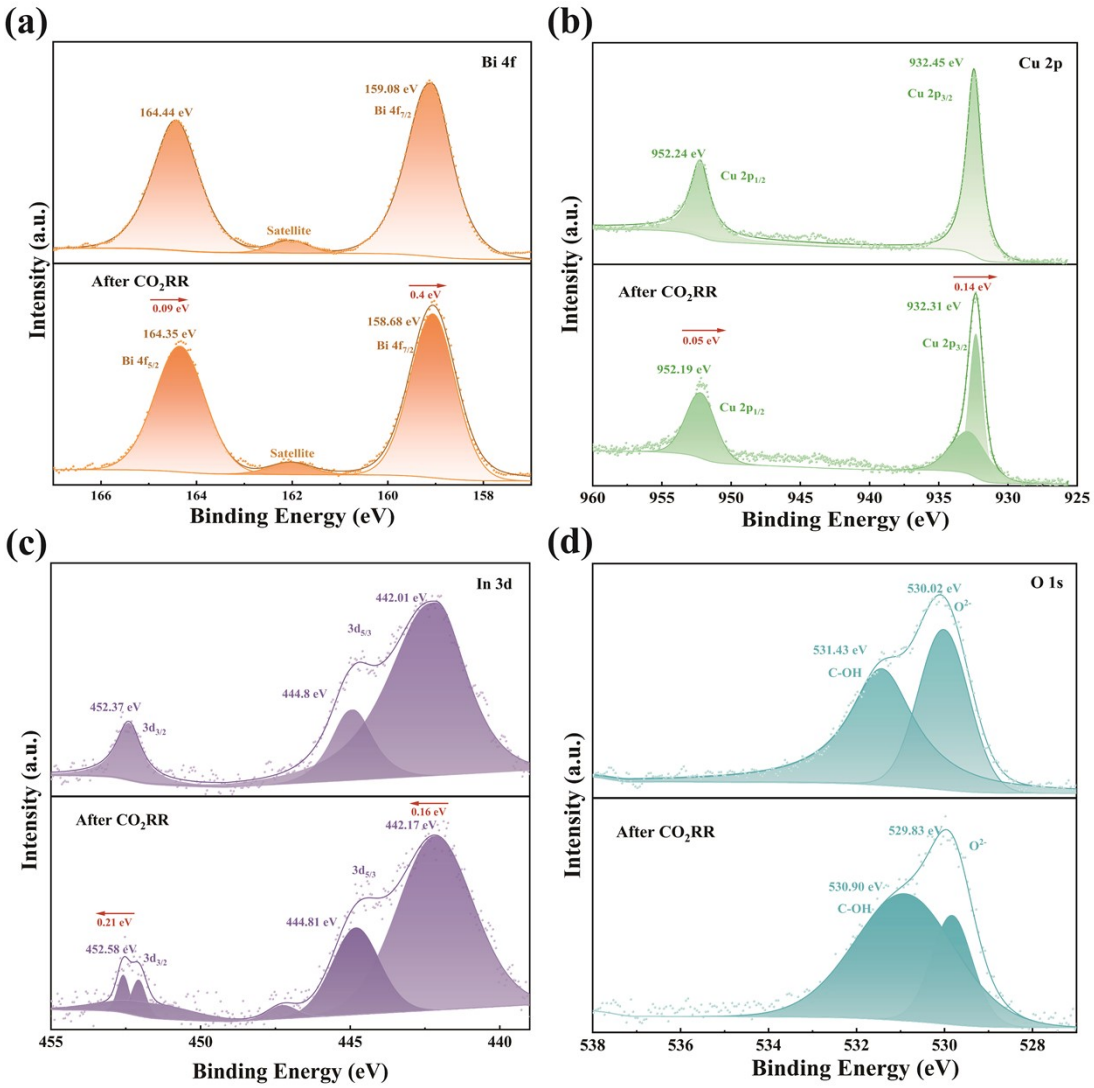


**Fig. S10** XPS spectra of $Bi_2O_3$-$In_2O_3$@CuO NWs before and after $CO_2$RR. (a) Bi 4f, (b) Cu 2p, (c) In 3d and (d) O 1s.

**Table S1** Comparison of electrocatalytic $CO_2RR$ to formate performance on various catalysts in H-cell from recent literatures.

| Catalysts | Electrolyte | Potential ($V_{RHE}$) | FE (%) | $J_{formate}$ (mA) | Formate rate (μmol $h^{-1}$) | Reference |
|---|---|---|---|---|---|---|
| **$Bi_2O_3$-$In_2O_3$ @CuO NWs** | **0.5 M $KHCO_3$** | **-0.75** | **88.7** | **28.4** | **529.5** | **This work** |
| | | **-0.85** | **83.7** | **33.5** | **624.5** | |
| | | **-0.95** | **69.2** | **31.8** | **593.7** | |
| Bi dendrite | 0.5 M $KHCO_3$ | -0.74 | 89.0 | 2.7 | / | [7] |
| Bi nanosheets | 0.1 M $KHCO_3$ | -1.10 | 86.0 | 16.5 | / | [8] |
| f- $Bi_2O_3$ | 0.1 M $KHCO_3$ | -1.20 | 87.0 | 20.9 | / | [9] |
| $Bi_2S_3$-$Bi_2O_3$ | 0.1 M $KHCO_3$ | -0.90 | 90.1 | 3.7 | / | [10] |
| $Bi_2O_3$@GO | 0.5 M $KHCO_3$ | -0.94 | 83.0 | 22.8 | / | [11] |
| $In_2O_3$@In-Co PBA | 0.1 M $KHCO_3$ | −0.96 | 85.0 | 13.5 | 135.7 | [12] |
| $SnInO_x$ | 0.1 M $KHCO_3$ | −1.30 | 80.0 | 24.0 | / | [13] |
| $Ag_{50}In_{50}$@$In_2O_3$ | 0.5 M $KHCO_3$ | −0.90 | 83.0 | 7.5 | 268.4 | [14] |
| InBDC | 0.5 M $KHCO_3$ | -0.67 | 88.0 | 6.8 | / | [15] |
| $In_{1.5}Cu_{0.5}$NPs | 0.1 M $KHCO_3$ | −1.20 | 90.0 | 3.9 | 214.3 | [16] |
| $Cu_2O$/Cu@NC | 0.1 M $KHCO_3$ | −0.68 | 70.5 | 4.3 | 188.7 | [17] |
| $Bi_2O_3$-$CuO_x$ | 0.5 M $KHCO_3$ | -0.76 | 89.3 | 8.2 | / | [18] |
| Cu NWs-BiNSs | 0.5 M $KHCO_3$ | -0.86 | 87.0 | 6.3 | / | [19] |

## References


1 C. Chen, J. F. Khosrowabadi Kotyk and S. W. Sheehan, *Chem*, 2018, **4**, 2571-2586.

2 J. Qiao, Y. Liu, F. Hong and J. Zhang, *Chem. Soc. Rev*., 2014, **43**, 631-675.

3 J. Li, S. U. Abbas, H. Wang, Z. Zhang and W. Hu, *Nanomicro Lett*., 2021, **13**, 216.

4 D. Xue, H. Xia, W. Yan, J. Zhang and S. Mu, *Nanomicro Lett*., 2020, **13**, 5.

5 Y. Zhao, X. Liu, Z. Liu, X. Lin, J. Lan, Y. Zhang, Y. R. Lu, M. Peng, T. S. Chan and Y. Tan, *Nano Lett*., 2021, **21**, 6907-6913.

6 D. Wu, J. Hao, Z. Song, X.-Z. Fu and J.-L. Luo, *Chem. Eng. J.*, 2021, **412**, 127893.

7 J. H. Koh, D. H. Won, T. Eom, N.-K. Kim, K. D. Jung, H. Kim, Y. J. Hwang and B. K. Min, *ACS Catal*., 2017, **7**, 5071-5077.

8 W. Zhang, Y. Hu, L. Ma, G. Zhu, P. Zhao, X. Xue, R. Chen, S. Yang, J. Ma, J. Liu and Z. Jin, *Nano Energy*, 2018, **53**, 808-816.

9 T. Tran-Phu, R. Daiyan, Z. Fusco, Z. Ma, R. Amal and A. Tricoli, *Adv. Funct. Mater*., 2019, **30**, 1906478.

10 X. Yang, P. Deng, D. Liu, S. Zhao, D. Li, H. Wu, Y. Ma, B. Y. Xia, M. Li, C. Xiao and S. Ding, *J. Mater. Chem. A*, 2020, **8**, 2472-2480.

11 B. B. Mulik, B. D. Bankar, A. V. Munde, A. V. Biradar and B. R. Sathe, *Chemistry*, 2020, **26**, 8801-8809.

12 J. Zhai, Q. Kang, Q. Liu, D. Lai, Q. Lu and F. Gao, *J. Colloid Interface Sci*., 2022, **608**, 1942-1950.

13 L. C. Pardo Pérez, D. Teschner, E. Willinger, A. Guiet, M. Driess, P. Strasser and A. Fischer, *Adv. Funct. Mater*., 2021, **31**, 2103601.

14 G. Wu, W. Chen, Y. Pang, R. Xie, D. Xia and G. Chai, *ChemElectroChem*, 2022, **9**, 2200318 .

15 S. Z. Hou, X. D. Zhang, W. W. Yuan, Y. X. Li and Z. Y. Gu, *Inorg. Chem*., 2020, **59**, 11298-11304.

16 B. Wei, Y. Xiong, Z. Zhang, J. Hao, L. Li and W. Shi, *Appl. Catal.*, B, 2021, **283**, 119646.

17 D. Li, T. Liu, Z. Yan, L. Zhen, J. Liu, J. Wu and Y. Feng, *ACS Appl. Mater. Interfaces*, 2020, **12**, 7030-7037.

18 C. Dai, Y. Qiu, Y. He, Q. Zhang, R. Liu, J. Du and C. Tao, *New J. Chem*., 2019, **43**, 3493-3499.

19 L. Li, F. Cai, F. Qi and D.-K. Ma, *J. Alloys Compd*., 2020, **841**, 155789.